ARMY RESEARCH LABORATORY

Host-dependence of Trivalent Erbium (Er^{3+}) Spectra Relevant to Solid-state Lasers: Yttrium Aluminum Garnet (YAG) and Sesquioxides

by Larry D. Merkle and Nikolay Ter-Gabrielyan

ARL-TR-5755 September 2011

NOTICES

Disclaimers

The findings in this report are not to be construed as an official Department of the Army position unless so designated by other authorized documents.

Citation of manufacturer's or trade names does not constitute an official endorsement or approval of the use thereof.

Destroy this report when it is no longer needed. Do not return it to the originator.

Army Research Laboratory
Adelphi, MD 20783-1197

ARL-TR-5755 **September 2011**

Host-dependence of Trivalent Erbium (Er^{3+}) Spectra Relevant to Solid-state Lasers: Yttrium Aluminum Garnet (YAG) and Sesquioxides

Larry D. Merkle and Nikolay Ter-Gabrielyan
Sensors and Electron Devices Directorate, ARL

REPORT DOCUMENTATION PAGE

Form Approved
OMB No. 0704-0188

1. REPORT DATE *(DD-MM-YYYY)*	2. REPORT TYPE	3. DATES COVERED (From - To)
September 2011	Final	May 2011

4. TITLE AND SUBTITLE

Host-dependence of Trivalent Erbium (Er^{3+}) Spectra Relevant to Solid-state Lasers: Yttrium Aluminum Garnet (YAG) and Sesquioxides

5a. CONTRACT NUMBER

5b. GRANT NUMBER

5c. PROGRAM ELEMENT NUMBER

6. AUTHOR(S)

Larry D. Merkle and Nikolay Ter-Gabrielyan

5d. PROJECT NUMBER

5e. TASK NUMBER

5f. WORK UNIT NUMBER

7. PERFORMING ORGANIZATION NAME(S) AND ADDRESS(ES)

U.S. Army Research Laboratory
ATTN: RDRL-SEE-M
2800 Powder Mill Road
Adelphi, MD 20783-1197

8. PERFORMING ORGANIZATION REPORT NUMBER

ARL-TR-5755

9. SPONSORING/MONITORING AGENCY NAME(S) AND ADDRESS(ES)

HEL-JTO
801 University Blvd SE Ste 209
Albuquerque NM 87106

10. SPONSOR/MONITOR'S ACRONYM(S)

11. SPONSOR/MONITOR'S REPORT NUMBER(S)

12. DISTRIBUTION/AVAILABILITY STATEMENT

Approved for public release; distribution unlimited.

13. SUPPLEMENTARY NOTES

14. ABSTRACT

The U.S. Army Research Laboratory is developing technologies for power-scalable solid-state lasers operating at cryogenic temperatures. We have particular interest in operation at wavelengths that present the least risk of ocular damage, resulting in considerable focus on trivalent erbium (Er^{3+}). We have carried out extensive comparisons of the spectra of Er^{3+} in two particularly promising types of oxide crystals: yttrium aluminum garnet (YAG) and various cubic sesquioxides. This report presents many of the principal results of this study. Er:YAG has more favorable properties for room-temperature laser operation, but some Er-doped sesquioxides appear more advantageous for operation at and near liquid nitrogen temperature.

15. SUBJECT TERMS

Erbium, eye safe, laser, YAG Y2O3, Sc2O3, sesquioxide, absorption, stimulated emission

16. SECURITY CLASSIFICATION OF:			17. LIMITATION OF ABSTRACT	18. NUMBER OF PAGES	19a. NAME OF RESPONSIBLE PERSON
a. REPORT	b. ABSTRACT	c. THIS PAGE			Larry D. Merkle
Unclassified	Unclassified	Unclassified	UU	38	19b. TELEPHONE NUMBER (*Include area code*) (301) 394-0941

Contents

List of Figures

Acknowledgments

We gratefully acknowledge financial support from the High Energy Lasers Joint Technology Office for portions of this work. We also acknowledge the valuable help of Arockiasamy Michael in taking some of the absorption spectra.

INTENTIONALLY LEFT BLANK.

Summary

The U.S. Army Research Laboratory (ARL) is developing technologies for power-scalable solid-state lasers operating at cryogenic temperatures. We have particular interest in operation at wavelengths that present the least risk of ocular damage, resulting in considerable focus on trivalent erbium (Er^{3+}). We have carried out extensive comparisons of the spectra of Er^{3+} in two particularly promising types of oxide crystals: yttrium aluminum garnet (YAG) and the cubic sesquioxides yttrium oxide (Y_2O_3), scandium oxide (Sc_2O_3), and (more briefly) lutetium oxide (Lu_2O_3). This report presents many of the principal results of this study. Er:YAG has more favorable properties for room-temperature laser operation, but some Er-doped sesquioxides appear more advantageous for operation at and near liquid nitrogen temperature. Compared to Er:YAG, their strongest long-wavelength absorption line are broader, making diode pumping at low temperature more feasible. They also have emission lines at wavelengths that afford great flexibility in the trade-off between very small quantum defect and minimum absorption at the laser wavelength.

INTENTIONALLY LEFT BLANK.

1. Introduction

Much of the military's research and development effort for high power or high energy lasers in recent decades has been focused on gas lasers driven by chemical reactions. Such systems were of interest because of their relatively easy scalability. However, they have certain key disadvantages. The gases are highly reactive, both the unreacted fuel gases and the reaction products are generally toxic, and they are sufficiently specialized to pose logistical challenges. Although more difficult to scale to high power, solid-state lasers are attractive for their avoidance of these problems. They are typically excited optically by electrically driven diode lasers. Since the requisite electricity can be generated by the power plant of the vehicle on which such lasers are mounted, the logistics trail is reduced to additional quantities of the fuel already required to power the vehicle.

As promising as solid-state lasers are, they pose substantial technical challenges. One is power efficiency, which has improved dramatically over the years but needs to increase further. Another is thermal management, since heat generated in the lasing process must exit a solid gain material by thermal conduction, unlike gas or liquid media that can be made to flow, carrying the thermal energy out of the laser cavity. Minimization of heating is important to reduce thermally induced optical distortions, since high beam quality is required for militarily useful lasers (and for many other applications).

Another challenge of importance for some applications of any high power laser is that of eye safety. In urban environments and even in some more open battlefield conditions, scattered light and stray reflections from targets can pose a substantial risk to the human eye.

The High Energy Lasers Team at ARL is investigating an interlocking set of approaches with great potential to meet these challenges. One is the use of crystalline or high quality ceramic laser media at cryogenic temperatures. This is promising because the thermal conductivities of such solids typically increase quite substantially as they are cooled from room temperature to the vicinity of 80–100 K (*1*). In addition, emission peaks typically become much narrower spectrally as the temperature is reduced, increasing the peak stimulated emission cross section (and thus the laser gain) proportionately, and the gain species' optical absorption at the laser wavelength is typically reduced by a large factor, reducing loss. Another of this set of approaches is the use of gain media that emit at wavelengths where the human eye is least susceptible to optical damage. The optimal region is about 1.3 to 2.5 microns (*2*). Combined with considerations of atmospheric transparency and the physics of realistic gain materials, this leads us to pay particular attention to laser ions such as Er^{3+} and trivalent holmium (Ho^{3+}). In particular, Er^{3+} has emission transitions between the manifolds $^4I_{13/2}$ and $^4I_{15/2}$ that can be made to lase at wavelengths around 1.5–1.6 microns, very near the optimum for eye safety, yet long

enough to avoid atmospheric carbon dioxide and water absorption peaks at about 1.3–1.5 microns.

Yet another of the interlocking approaches being pursued is the optical pumping of the laser material by diode lasers at a wavelength as close as possible to the material's laser wavelength. This gives an extremely small "quantum defect," meaning that the absorbed pump photon has only slightly more energy than the emitted laser wavelength, so that very little of the pump photon's energy is deposited in the gain medium as heat. This approach has been demonstrated by our own group and others for several laser ions, notably trivalent ytterbium (Yb^{3+}), Er^{3+}, and Ho^{3+} (*3–6*). The diode lasers at wavelengths suited to pump Yb^{3+} are particularly efficient, but that ion emits at wavelengths where the eye is quite sensitive to damage. Er^{3+} and Ho^{3+} are far superior for eye safety, but the diode lasers operating in the corresponding wavelength ranges, around 1.5 microns and 2 microns, respectively, are less mature and semiconductor physics indicates that they will never be as efficient as their shorter-wavelength analogs. Between these two wavelength ranges, diode lasers at and near 1.5 microns have somewhat higher efficiency, increasing our interest in Er^{3+}.

The research covered in this technical report addresses Er^{3+} in the crystalline or ceramic hosts yttrium aluminum garnet (YAG, or $Y_3Al_5O_{12}$,) Y_2O_3, Sc_2O_3, and Lu_2O_3. YAG is one of the more robust and successful host materials used for gain media, whereas the sesquioxides have somewhat higher thermal conductivity (*7, 8*). We wish to determine which of these materials has the most favorable spectroscopic properties for laser operation, particularly at cryogenic temperatures.

2. Methods – Experimental

Absorption spectra were taken using a Varian Cary 6000i ultraviolet-visible-near infrared (UV-vis-nIR) spectrophotometer, which uses an indium gallium arsenide (InGaAs) detector for the nIR portion of the spectral range. The highest (that is, narrowest,) spectral resolution of this instrument is about 0.07 nm, and the resolution typically employed was 0.1 nm. For very narrow absorption features in the 1510–1630 nm range, a Santec TSL-210V tunable diode laser with a bandwidth of about 1 pm (0.001 nm) was used, its transmission being monitored as its wavelength was scanned across the peaks of interest.

Fluorescence spectra were taken using an Acton SpectraPro 2500i monochromator. The spectral bandwidth was typically 0.15 nm, and detection was by either liquid nitrogen cooled or thermoelectrically cooled InGaAs detectors. Spectra were corrected for the spectral response of the detection system. Continuous wave (CW) diode lasers with wavelengths near 980 nm were used for excitation.

For fluorescence lifetimes, excitation was accomplished either by pulsing one of the diode lasers or by a SEO Titan P pulsed titanium (Ti):sapphire laser. A shorter focal length monochromator was typically used, to improve the throughput, and the resulting decay signal from one of the InGaAs detectors was recorded using a Tektronix TDS7104 digitizing oscilloscope.

3. Methods – Analysis

Much of the information sought in this study can be embodied in spectra of the ground state absorption and stimulated emission cross sections of transitions between the $^4I_{15/2}$ ground manifold and $^4I_{13/2}$ first excited manifold of Er^{3+} in each host. The absorption cross section spectra were obtained from the observed absorption spectra using the full measured Er concentration for YAG, but only three-quarters of the measured value for the sesquioxides. This was done because that class of hosts has two distinct cation sites that can host a trivalent rare earth ion, three-quarters of which have C_2 site symmetry and the other one-quarter C_{3i} symmetry (*9–11*). Due to the inversion symmetry of the C_{3i} site, electric dipole transitions are forbidden for Er ions in that type of site, resulting in spectra that are generally weaker than for Er in the C_2 site. The above-noted concentration scaling for the sesquioxides amounts to a two-fold assumption: that the Er ions occupy these two types of sites randomly so that the proportion of Er ions on each matches the proportion of sites available and that transitions from the C_2 sites dominate the spectra. The former assumption should be quite sound for Y_2O_3 and Lu_2O_3, owing to the very similar ionic radii of Er^{3+},Y^{3+}, and Lu^{3+}, but is less certain for Sc_2O_3 due to a more substantial size mismatch in that case (*12*). The latter assumption is just an approximation, as magnetic dipole transitions can have significant strength, and thus some lines from Er in the C_{3i} site may appear in the spectrum. If they do, our approach understates their strength by approximately a factor of three.

Stimulated emission spectra were obtained in two ways. The McCumber or reciprocity method, which relies on the reciprocity of absorption and stimulated emission transitions between any two energy levels, infers the stimulated emission cross section at a given wavelength from the absorption cross section (*13*). This relation may be written

$$\sigma_{se}(\lambda) = \sigma_a(\lambda)\,(Z_l/Z_u)\,\exp[(E_0 - hc/n\lambda)/k_BT]. \quad (1)$$

Here $\sigma_{se}(\lambda)$ and $\sigma_a(\lambda)$ are the stimulated emission and absorption cross sections, respectively, at wavelength λ; Z_l and Z_u are the partition functions for the lower and upper manifolds, respectively; E_0 is the energy difference between the lowest states of the two manifolds (called the ~~z~~ero line"); h is Planck's constant; c is the speed of light in vacuum; n is the index of refraction of the medium in which the wavelength is measured (air in our case); k_B is Boltzmann's constant; and T is the temperature. The other method for obtaining stimulated emission cross-section spectra is due to Fuchtbauer and Ladenburg, which obtains its result from

measured fluorescence spectra. The derivation is given nicely in Aull and Jenssen (*14*), with the resulting equation given here after removing an extraneous factor from their equation:

$$\sigma_{se}(\lambda) = \eta\, \lambda^5\, I(\lambda) / 8\pi n^2 c\, \tau_f\, (\int \lambda' I(\lambda') d\lambda'). \quad (2)$$

Here η is the quantum efficiency of the emission, including the branching ratio if the upper manifold decays to more than one lower manifold; $I(\lambda)$ is the fluorescence intensity at wavelength λ; n is the index of refraction in the material; τ_f is the observed fluorescence lifetime; and the integral is over the entire emission band (in the present case, the Er^{3+} $^4I_{13/2} \rightarrow {}^4I_{15/2}$ emission). Thus, τ_f / η is the radiative lifetime of the upper level. The indices of refraction for the materials reported here were taken from the following sources: Zelmon et al. for YAG, the Handbook of Optics for Y_2O_3, Mix for Sc_2O_3, and Medenbach et al. for Lu_2O_3 (*15–18*).

Each of these methods has significant sources of error, but those sources are entirely different, so that each method can serve as a check of the other. In the McCumber (reciprocity) approach, the concentration must be known accurately to get the absorption cross-section spectrum, and the energy levels must be known to calculate the partition functions accurately. In the Fuchtbauer-Ladenburg (F-L) method, the quantum efficiency must be known, or equivalently, it must be known how the observed fluorescence lifetime relates to the radiative lifetime of the upper manifold. Also, sufficiently thin samples with sufficiently low dopant concentration must be used to minimize reabsorption of the fluorescence, which can cause problems, as described in the next section.

4. Comparison of the Overall $^4I_{15/2} \leftrightarrow {}^4I_{13/2}$ Spectra

Many of the relative spectroscopic strengths and weaknesses of the laser materials under study can be discerned simply by comparing their absorption and emission spectra in the spectral region around 1.5 microns, that is, the region of the $^4I_{15/2} \leftrightarrow {}^4I_{13/2}$ transitions (*19*).

Figure 1 shows the room-temperature absorption (ground-state absorption [GSA]) and stimulated emission (SE) spectra of the $^4I_{15/2} \leftrightarrow {}^4I_{13/2}$ transitions in Er:YAG. The SE spectrum uses reciprocity results at short wavelengths and F-L results at long wavelengths to take advantage of the strengths of each method and minimize each one's weaknesses. The strongest absorption peaks are those near 1530 nm. They are useful for diode pumping, since their relatively long wavelengths minimize quantum defect, but they are rather narrow, thus requiring spectral narrowing of the diode laser emission for efficient pumping. The absorption peaks between 1450 and 1475 nm are somewhat weaker and their shorter wavelengths result in larger quantum defects, but they are broad enough to absorb diode pump light efficiently with little or no need of spectral narrowing. The strongest emission lines overlap strong absorptions near 1530 nm and thus are useless for lasing, but there are very satisfactorily strong emission lines between 1617 and 1660 nm (stimulated emission cross sections of $5\text{-}6\times10^{-21}$ cm^2) that have little absorption to

overcome to reach laser threshold. Er:YAG has been lased on these transitions by a number of groups, some using laser pumping and others the potentially simpler and more efficient method of diode pumping (*5, 20–26*).

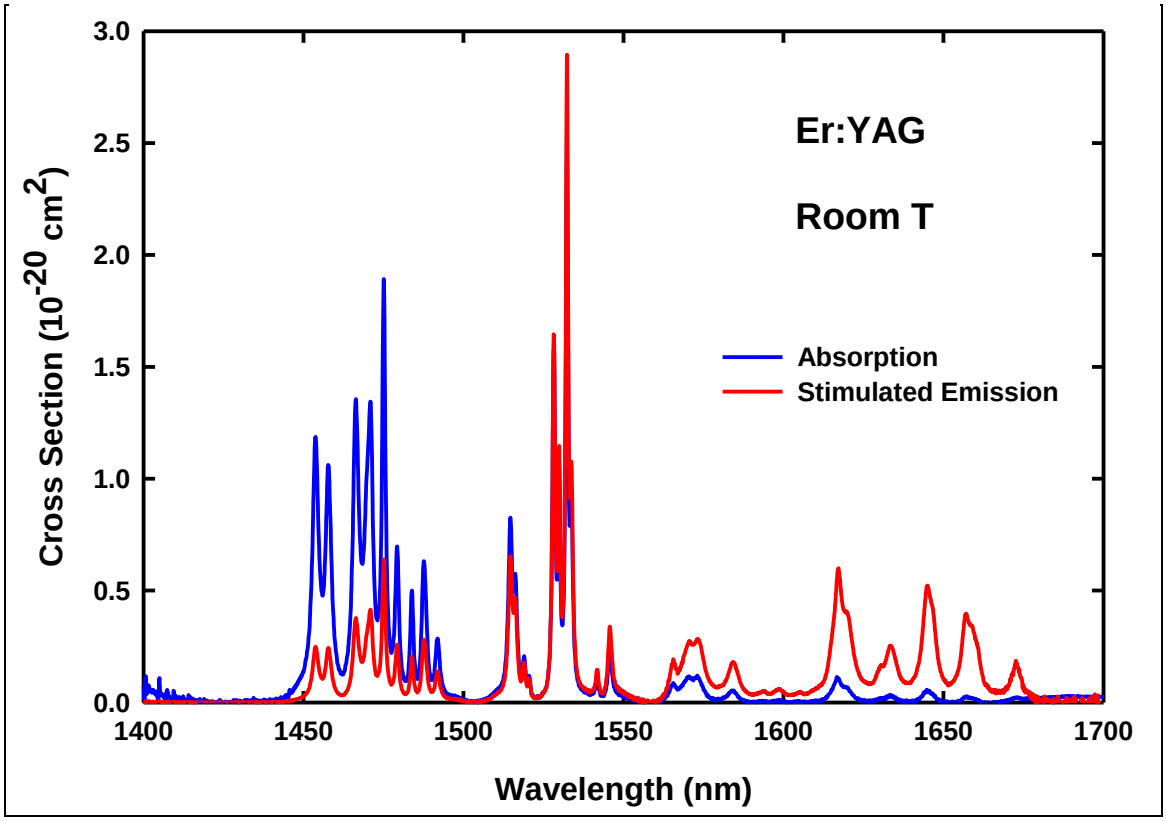

Figure 1. Absorption (blue) and stimulated emission (red) spectra of Er:YAG at room temperature.

There are important differences between these room-temperature spectra and the corresponding spectra at liquid nitrogen temperature, as seen in figure 2. Many transitions are narrower, the laser lines noted above are stronger due to this line-narrowing, and the absorption at the laser wavelengths is much smaller, all as expected at cryogenic temperatures. Of more interest for the present work, the absorption and emission transitions between 1550 and 1600 nm have disappeared, as they originate on sufficiently high-lying energy levels to have insignificant thermal population at 77 K (*27, 28*). As a result, although it would generally be attractive to take advantage of the reduced absorption to use shorter-wavelength emission lines at cryogenic temperatures, this is not practical for Er:YAG. We attempted to lase the transition at 1546 nm, but found that its absorption is too strong even at this temperature. Thus, despite the favorable features of Er:YAG as a laser at 1617 nm and longer wavelengths with moderately small quantum defect, it is not an attractive candidate for very small quantum defect laser operation.

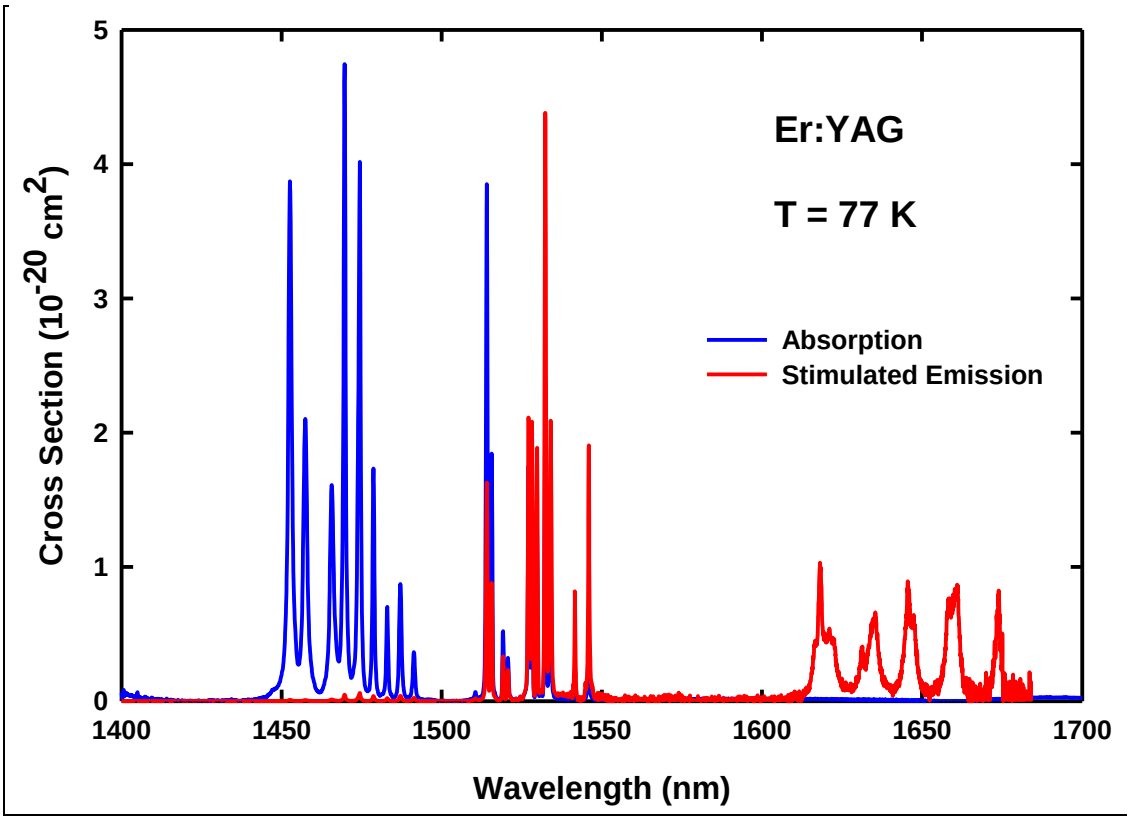

Figure 2. Absorption (blue) and stimulated emission (red) spectra of Er:YAG at 77 K.

The relationship between the observed Er:YAG fluorescence lifetime and the calculation of the stimulated emission cross-section spectrum by F-L is worthy of comment. We have found that for samples with any significant Er concentration, even as little as 0.5% atomic (with respect to the Y concentration), radiative reabsorption is significant. In this phenomenon, a photon emitted as fluorescence from one ion is absorbed by another, which then decays in accordance with the radiative lifetime except that its —zero" of time is reset at the moment of absorption. This combination of ions whose decay dynamics begin from a wide range of start times results in the observed lifetime being stretched compared to the true radiative lifetime. If sufficient samples are available of a given material to sacrifice at least one, as was true for Er:YAG in this study, it can be ground to fine powder, pressed in a thin layer so that fluorescence encounters as few Er^{3+} ions as possible, and lifetimes measured on such a sample. For powdered 0.5% Er:YAG, the resulting observed lifetimes decreased from 9.9 ms at 77 K to 7.3 ms at room temperature. However, using these values as radiative in equation 2, that is, assuming $\eta=1$ so that τ_f becomes $\tau_{radiative}$, results in stimulated emission spectra from F-L whose magnitudes do not match those from reciprocity. Scaling the F-L result to match the reciprocity result in the wavelength range where both are useful and then using the full spectrum and equation 2 to predict the radiative lifetime gives radiative lifetimes of 5.9 and 6.5 ms at 77 K and room temperature, respectively. This suggests that even our fluorescence decay measurements on a fairly thin layer of powder were affected significantly by reabsorption.

The spectral characteristics of Er-doped sesquioxides present quite different strengths and weaknesses for laser operation near 1.5 microns. The room-temperature absorption and emission of Er:Y_2O_3 (figure 3) show that the emission lines beyond 1600 nm (that is, the transitions that have little absorption to overcome even at room temperature) are much weaker than those in Er:YAG, with cross sections of only ~1.1–1.3×10^{-21} cm^2. This considerably reduces this material's promise as a room-temperature eye-safe laser in this wavelength regime. There is one compensating advantage; however, namely, that the strongest absorption line, at about 1535 nm, is much broader than the corresponding line in Er:YAG. This greatly reduces the need for spectral line narrowing of pump laser diodes.

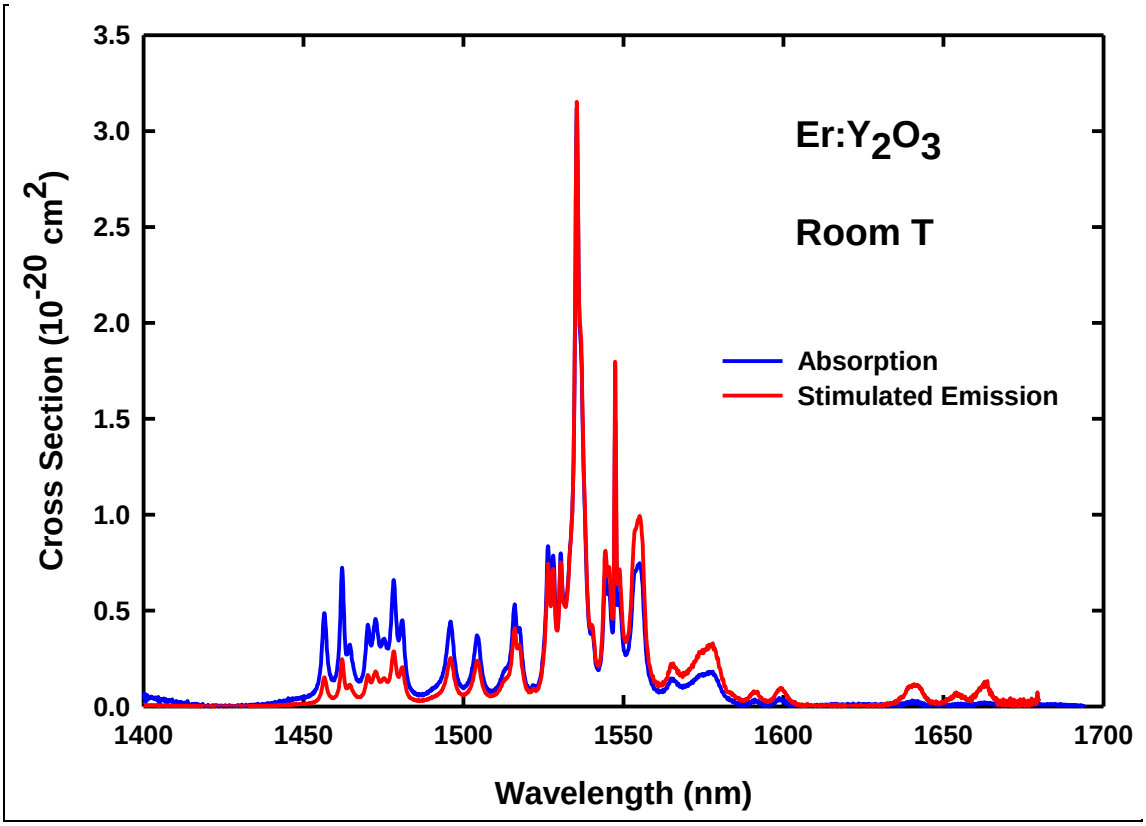

Figure 3. Absorption (blue) and stimulated emission (red) spectra of Er:Y_2O_3 at room temperature.

Whereas the potential gain lines in Er:Y_2O_3 are much weaker than those in Er:YAG at room temperature, the situation is very different at 77 K, as can be seen in figure 4. The emission lines beyond 1600 nm remain quite weak, but the distribution of energy levels in Er:Y_2O_3 is such that there exist substantial emission lines at 1574 and 1600 nm, the region in which Er:YAG has no useful lines at cryogenic temperatures. These lines in Er:Y_2O_3 have little absorption at 77 K and stimulated emission cross sections very comparable to those of the longer-wavelength lines in Er:YAG. The shorter wavelengths of these Er:Y_2O_3 lines make them quite promising for very small quantum defect lasing at this temperature—much more so than any line in Er:YAG.

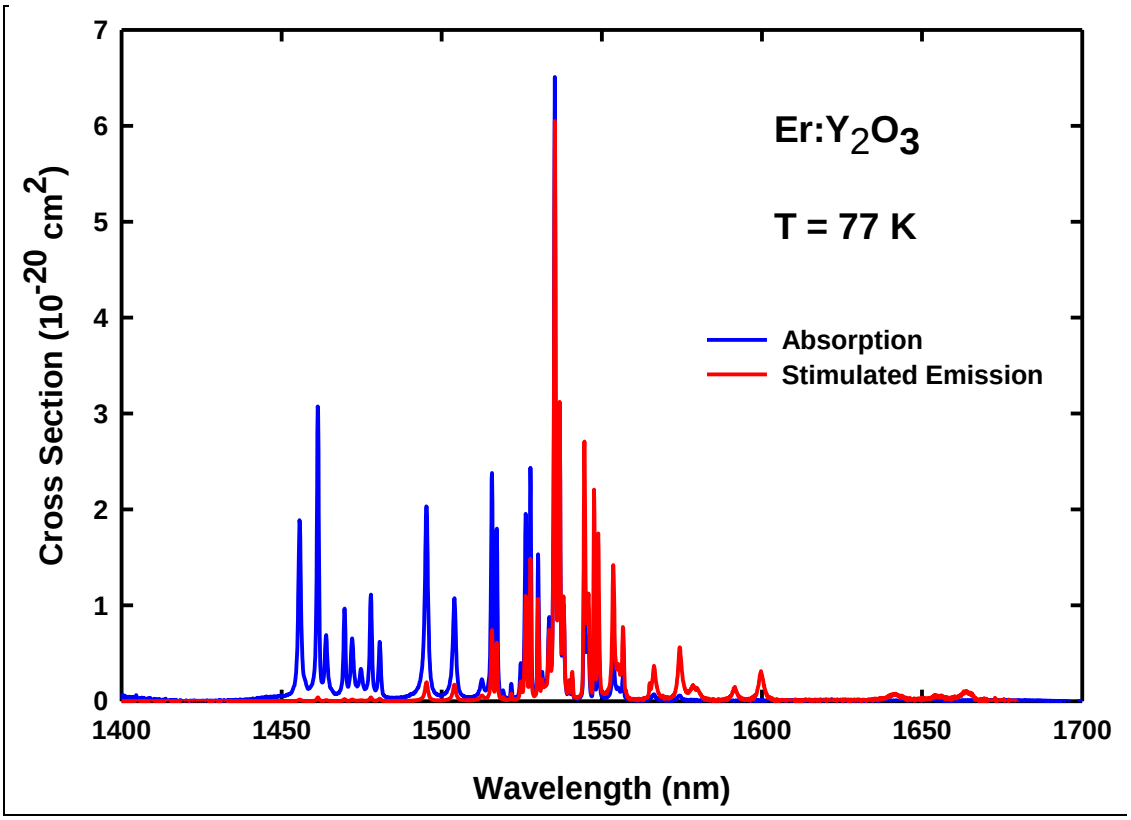

Figure 4. Absorption (blue) and stimulated emission (red) spectra of Er:Y_2O_3 at 77 K.

This advantage of Er-doped Y_2O_3 for cryogenic lasing with extremely small quantum defect also exists for Er in other sesquioxides, with some interesting differences of detail. Figures 5 and 6 show the room temperature and 77 K absorption and stimulated emission spectra of Er:Sc_2O_3. Not surprisingly for two hosts with the same structure, the pattern of lines is similar to that in Y_2O_3. However, the various lines are generally split more widely in Er:Sc_2O_3, suggesting that the crystal field at that material's Er sites (and particularly at the C_2 site whose transitions dominate the spectra in both hosts) is stronger in Sc_2O_3 than in Y_2O_3. This is probably attributable to the ionic size of Sc^{3+} being smaller than that of Y^{3+}, so that the neighboring oxygens are somewhat closer to Er^{3+} Sc_2O_3 (*12*). At room temperature, the main effect of this difference is to shift the exact wavelengths of the potential laser lines, which remain so much weaker than in Er:YAG that the latter probably remains more promising for room-temperature lasing than either Er-doped sesquioxide. However, the effect of the larger crystal field splitting is more interesting at liquid nitrogen temperature. The emission lines offering the possibility of very small quantum defect lasing are at somewhat longer wavelengths in Er:Sc_2O_3 than in Er:Y_2O_3, with the line at 1574 nm in the latter shifted to 1581 nm in the former, for example. This makes the potential quantum defect somewhat poorer (larger) in Er:Sc_2O_3, but it also makes the absorption of each such line smaller relative to the stimulated emission. For practical laser operation, this reduced absorption may more than offset the slightly poorer quantum defect.

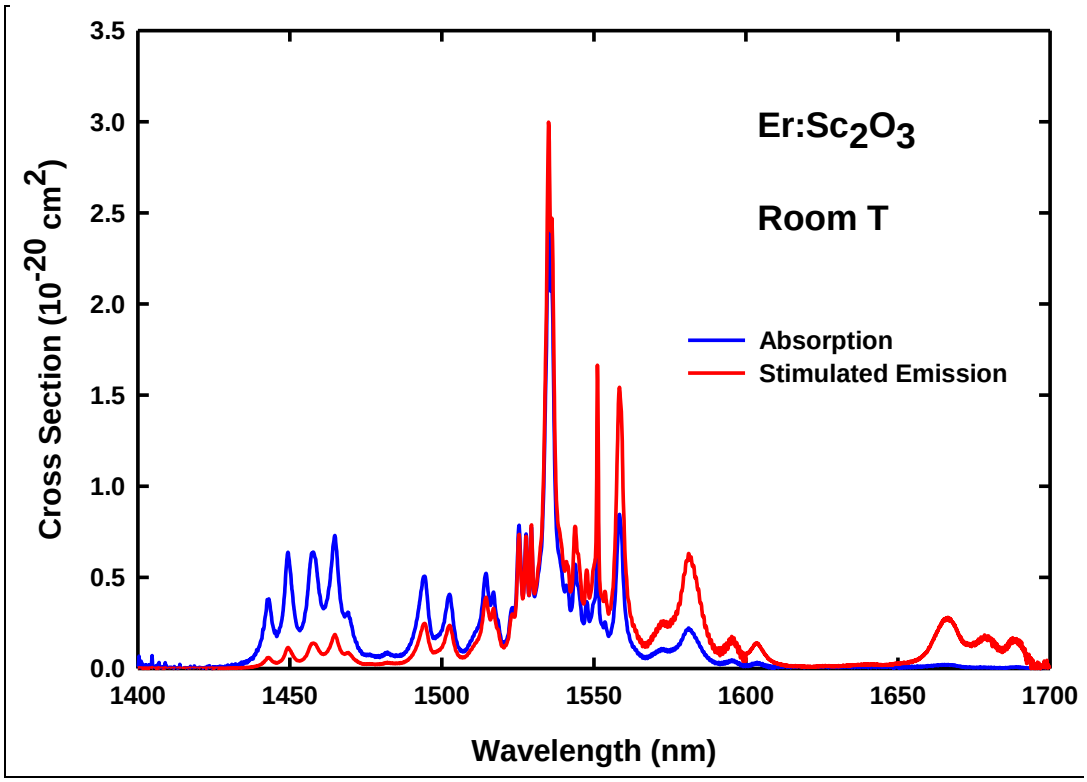

Figure 5. Absorption (blue) and stimulated emission (red) spectra of $Er:Sc_2O_3$ at room temperature.

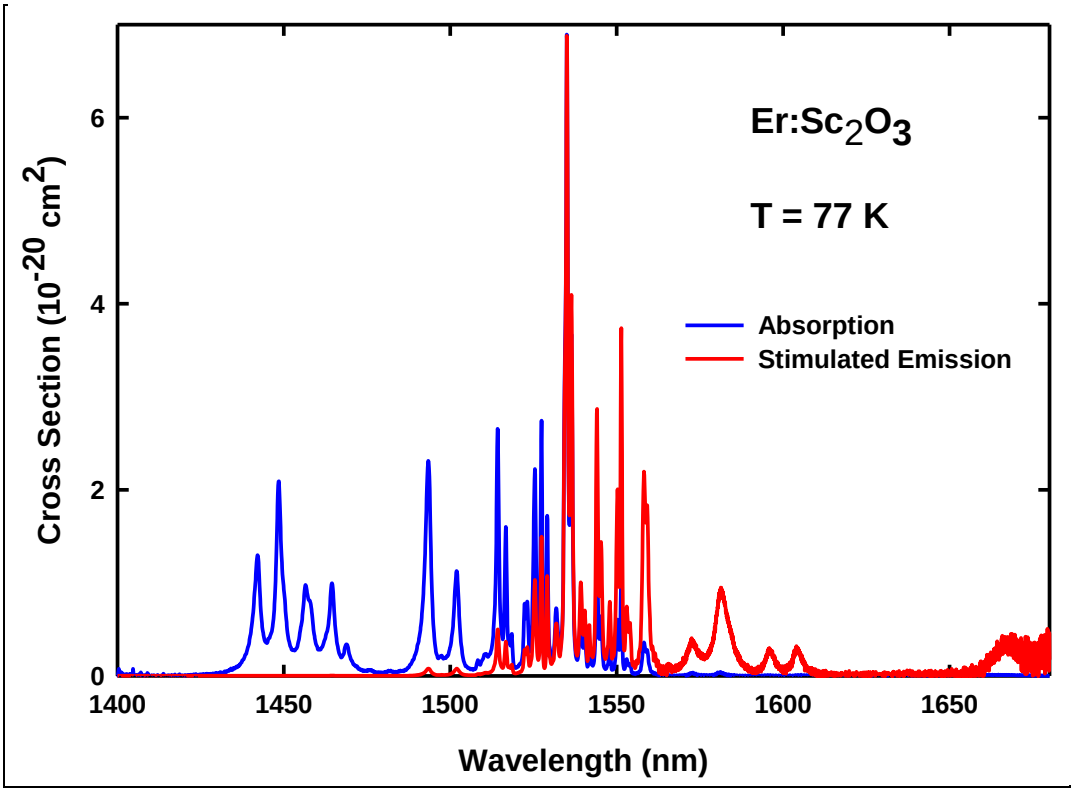

Figure 6. Absorption (blue) and stimulated emission (red) spectra of $Er:Sc_2O_3$ at 77 K.

As for Er:YAG, one must be cautious regarding the effect of reabsorption on the observed lifetimes used in the F-L method for obtaining stimulated emission cross sections in Er-doped sesquioxides. In our Er:Y_2O_3 study, we observed a room-temperature lifetime much longer than was reported in the literature, leading us to suspect that reabsorption had a large effect. Thus, for our F-L calculations, we relied on other groups' lifetime values: 7.6 ms at room temperature, reported by Laversenne et al. (*29*), and 10.5 ms at 77 K, a preliminary result from colleagues at the MIT Lincoln Laboratories (*30*). As for Er:YAG, we have combined the stimulated emission spectra of Er:Y_2O_3 obtained from absorption by reciprocity and from fluorescence by F-L theory, and have used the result and equation 2 to infer the radiative lifetime at each temperature. The resulting values are 5.0 ms at room temperature and 7.9 ms at 77 K—each significantly shorter than the observed value. Unless the Er concentration in the sample is incorrect, this strongly suggests that these reported values are affected by reabsorption. We have confidence in the Er concentration based on comparison of the absorption with that of a sample subsequently analyzed chemically for Er. For Er:Sc_2O_3, we measured fluorescence lifetimes on a powdered sample to minimize the effect of reabsorption, observing values of 6.9 ms at 77 K and 6.2 ms at room temperature. The values inferred from the combined reciprocity and F-L stimulated emission spectra are 5.5 and 5.0 ms, respectively. Since the estimated uncertainties in both the observed and calculated lifetimes are approximately 10%, it is just possible that these values are consistent. It is, however, more probable that even our powder lifetime data are affected somewhat by reabsorption, though not as strongly as in the other materials.

We have also performed spectroscopic studies of Er:Lu_2O_3, but these studies have thus far been more limited, due to sample availability and quality. Acting for the present on the assumption that our observed powder lifetime measurements, 10.5 ms at 77 K and 8.5 ms at room temperature, are useful approximations to the radiative lifetimes, we have calculated the stimulated emission spectra by the F-L method. The results are shown in figure 7. Although our experience with the observed lifetimes in the other materials suggests that the results be viewed with caution, the spectra are reasonable. In particular, the strongest lines at ~1580 nm and longer wavelengths have peak cross sections roughly consistent with those of Er:Y_2O_3 and Er:Sc_2O_3.

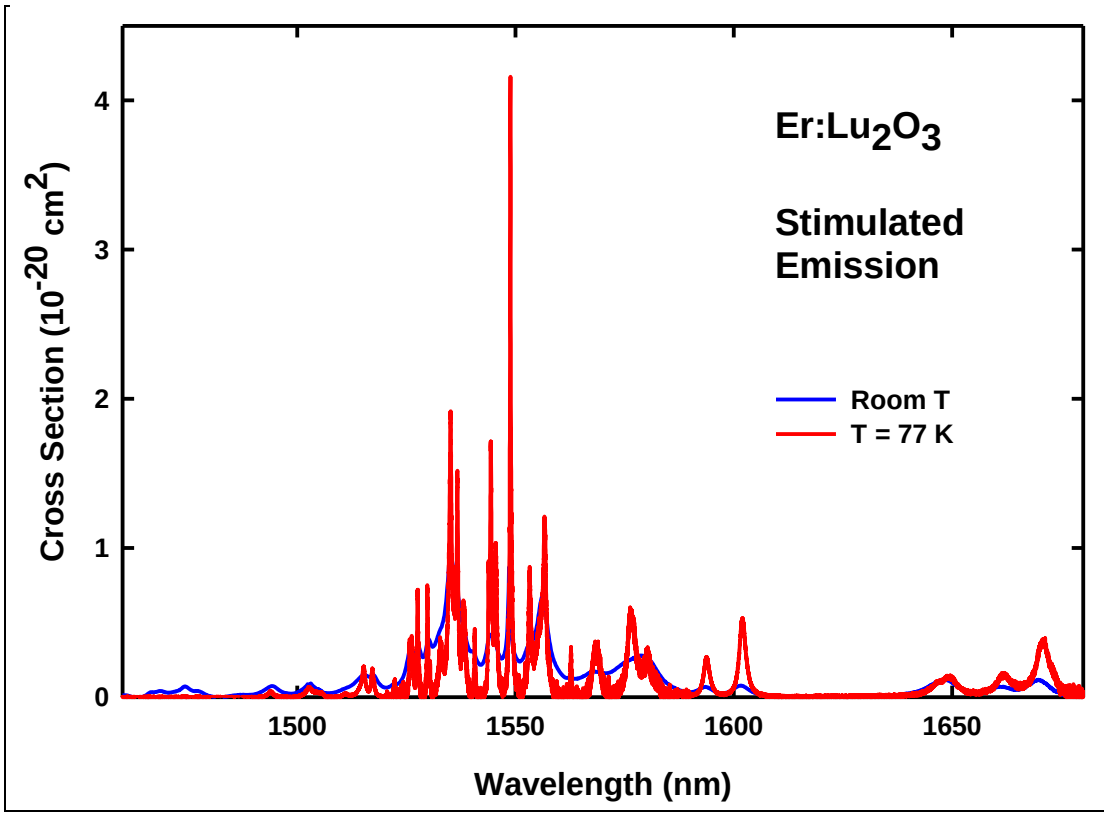

Figure 7. Stimulated emission spectra of Er:Lu_2O_3 at 77 K (red) and room temperature (blue). These were obtained by the F-L method, assuming the observed lifetimes to be radiative.

5. Er:YAG Detail – the 1546-nm Absorption Peak

As noted in the preceding section, it is desirable to reduce the quantum defect between the energies of the pump and laser photons as much as possible, consistent with choosing a laser wavelength long enough to have low absorption. Due to the large gap in the emission spectrum of Er:YAG at 77 K (figure 2), it is not realistic to choose a laser wavelength shorter than that of the 1617-nm peak. The next shorter-wavelength significant peak, at 1546 nm, has such a large absorption cross section, approximately 7×10^{-21} cm^2, that the laser threshold would be too high for good efficiency. However, this substantial absorption presents a new possibility for reducing the quantum defect: the use of this line for pumping. Pumping at 1546 nm and lasing at 1617 nm gives a quantum defect of 4.6%, significantly smaller than the 5.5% quantum defect achieved with the same laser line by pumping the strong absorption line at 1532 nm. It must be noted that the peak absorption cross section of the 1532-nm line at 77 K is fully two orders of magnitude larger, but it is also much narrower (0.019 nm full width at half maximum for the 1532-nm peak vs 0.7 nm for the 1546-nm peak) (*31*). Thus, for diode pumps of realistic spectral width, the breadth of the 1546-nm absorption line largely compensates for its smaller peak cross

section and enables fairly good absorption. Tests verify that laser operation with 1546-nm pumping is as efficient as with 1532-nm pumping if calculated on the basis of absorbed pump power, and that the fraction of the incident pump power absorbed is reasonable (*31*). That fraction can be optimized by selection of the gain medium's length.

6. $Er:Sc_2O_3$ and $Er:Y_2O_3$ Detail – Temperature Dependence of the $Er:Sc_2O_3$ 1558-nm Laser Line

As noted in the section on the overall spectra, $Er:Sc_2O_3$ has the potential to lase on the 1581-nm line at cryogenic temperatures. Members of our group have observed that in some circumstances lasing occurs on the even lower quantum defect line at 1558 nm (*32*). This can be achieved by use of a wavelength selective cavity mirror that strongly favors 1558 nm over 1581 nm, or by choosing the output coupler loss appropriately. Intriguingly, with output coupling that favors 1581 nm at 77 K, laser action spontaneously switches to 1558 nm as the temperature is increased above approximately 110 K. This is counterintuitive, since the ratio of absorption to stimulated emission cross section is larger at shorter wavelengths and gets larger still as the temperature is increased. Increasing absorption cross sections, along with decreasing stimulated emission due to line broadening as the temperature increases, tends to increase laser threshold. Thus, one usually finds that any switch of laser wavelength with increasing temperature will be to longer wavelength. Ter-Gabrielyan et al. (*33*) were able to show that lasing at 1558 nm in $Er:Sc_2O_3$ involves relatively high-lying initial and final energy levels, and that this successfully predicts the shift to shorter wavelength in this material. Here, we look in somewhat more detail at the spectra of $Er:Sc_2O_3$ and $Er:Y_2O_3$ to further clarify this phenomenon.

Figure 8 shows the temperature dependence of the $Er:Sc_2O_3$ absorption features near 1560 nm and of the stimulated emission cross-section spectra derived from the absorption. Whereas one often sees the stimulated emission peak height decrease with temperature due to line broadening, in this case, the peak remains practically constant until the temperature exceeds 150 K. In seeking an explanation for this, it is worthwhile to note from the shape of the spectrum that there are at least two overlapping transitions at and near 1558 nm. In fact, published energy levels for Er^{3+} in the C_2 site of Sc_2O_3 indicate that there are three transitions at very nearly the same photon energy, noted in figure 9 (*34*). This suggests that the robust strength of the 1558-nm peak is due to thermal excitation of a transition that is strong enough for its growing role to counteract the effect of line broadening.

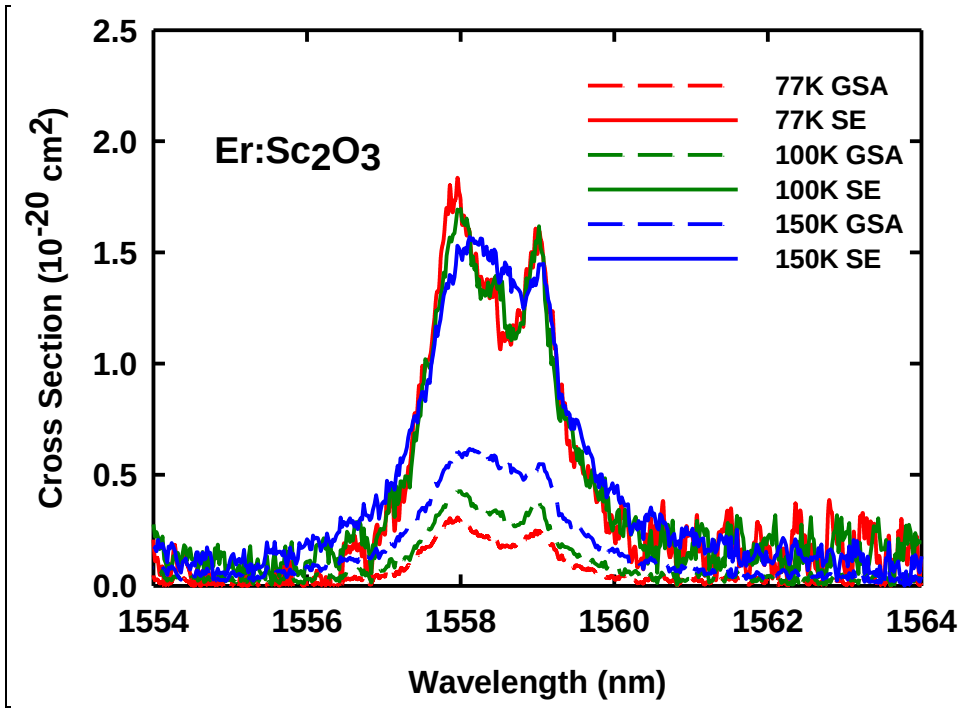

Figure 8. Temperature-dependent Er:Sc_2O_3 absorption cross section and stimulated emission cross-section spectra derived via reciprocity around the feature responsible for 1558-nm laser action.

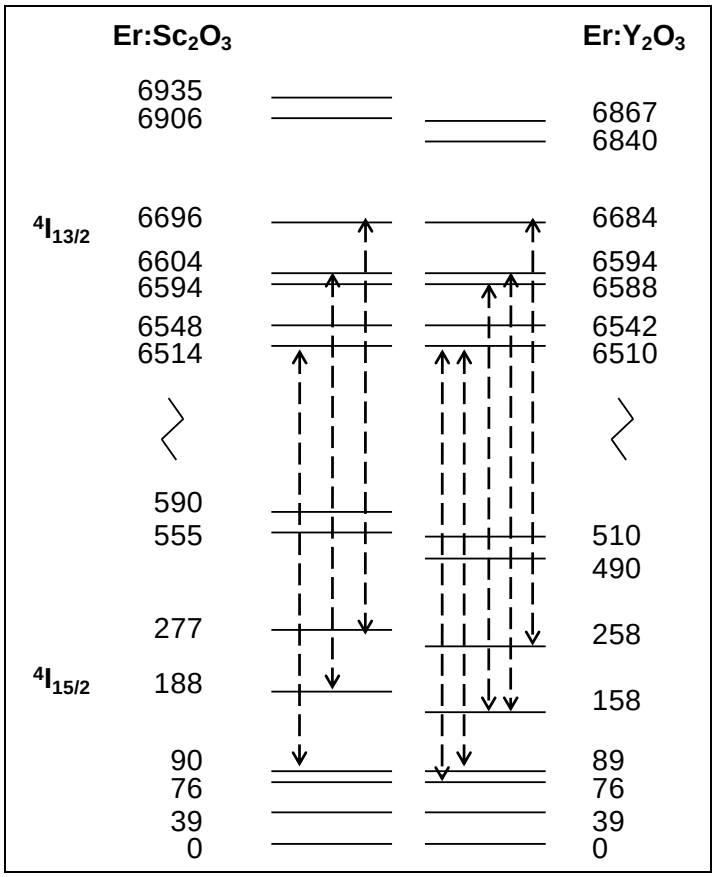

Figure 9. Relevant C_2 $^4I_{15/2}$ and $^4I_{13/2}$ energy levels of Er:Sc_2O_3 (left) and Er:Y_2O_3 (right), showing the transitions that contribute to spectra near 1550–1560 nm.

It is helpful to look at the transitions of Er:Y_2O_3 at about the same wavelength to sort out the effects of different transitions. As shown in figure 10, the transitions are better separated in Er:Y_2O_3, and there are more transitions in this region. Indeed, figure 9 shows that there are fully five transitions among states of Er^{3+} in the C_2 site in this region (*10*). Close scrutiny of the absorption spectra for temperatures from 20 K through room temperature show all five of the transitions, with peak wavelengths of approximately 1553.2, 1553.5, 1554.3, 1555.0, and 1556.5 nm. These values are inexact, due in part to their being incompletely resolved and in part to the fact that even rare earth $4f^N$ energy levels, shielded from the lattice though they are, shift somewhat with temperature. As the temperature is increased from the minimum, the 1553.5-nm, line appears first, and both it and the 1556.5-nm line are already rather strong by 50 K. The 1553.2-, and 1555.0-nm lines are clear but weak at 50 K and are not discernable below that temperature. All these are narrow at low temperatures, near 0.1 nm at 50 K, for example. The 1554.3-nm line behaves rather differently. It is barely discernable at 50 K but grows much more strongly than the other lines as the temperature increases. It is also several times the width of the other lines up through about 100 K, beyond which thermal broadening of the other lines reduces that difference. Although thermal broadening makes it progressively more difficult to fit

individual peak widths and heights reliably as the temperature increases, it appears that the transitions at 1554.3 and 1555.0 nm have the greatest strengths at temperatures above roughly 150 K.

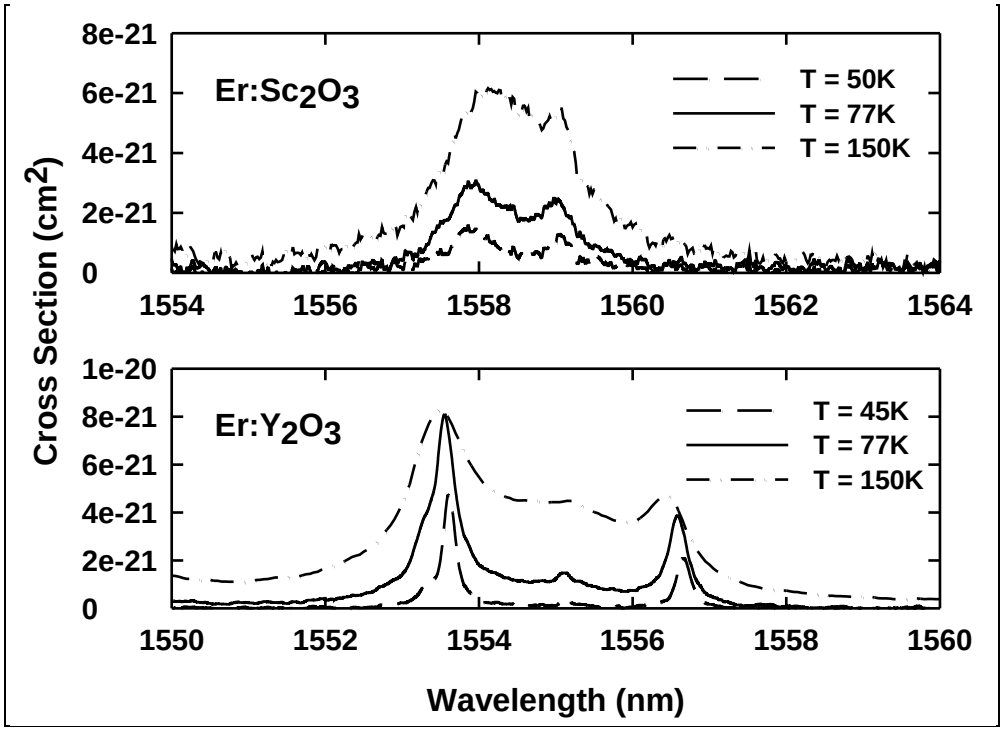

Figure 10. Comparison of the temperature-dependent absorption spectra of Er:Sc_2O_3 and Er:Y_2O_3 near 1550–1560 nm.

These trends make sense in light of the energies in figure 9. Transitions from the third and fourth levels of $^4I_{15/2}$ should have appreciable thermal population at lower temperatures than the others, and their initial states for absorption are so similar in energy that they should grow similarly with temperature. Of those two, the one with the lower initial state has the second largest photon energy of the five, and the other has the smallest. This is consistent with the behaviors of the 1553.5- and 1556.5-nm lines. The next two transitions in this wavelength range to achieve appreciable thermal population would be those originating on the fifth level of $^4I_{15/2}$, one of which has the largest photon energy of the five. These are consistent with the transitions observed at 1553.2 and 1555.0 nm. The remaining transition, originating on the sixth level of $^4I_{15/2}$, should reach appreciable thermal population only at a higher temperature than the others, but should grow more strongly than the rest at higher temperatures, consistent with the transition at 1554.3 nm. Also, since transitions involving high-lying states in $4f^N$ manifolds are very often much wider than transitions involving only low-lying states, the much greater width of that transition is not surprising.

These patterns in Er:Y_2O_3 indicate that similar behavior can be expected in Er:Sc_2O_3, though the stronger overlap of the three relevant transitions makes the sorting out of the temperature

dependence and line strengths much more difficult. Indeed, the best way to evaluate these is to integrate the absorption cross section under the entire 1555–1562-nm set of peaks, plot this ~~–a~~rea" as a function of temperature, and fit it to a sum of effective transition strength terms corresponding to the initial states of the three transitions (the states at 90, 188, and 277 cm^{-1} in figure 9). Each term is comprised of a constant prefactor multiplying a thermal population factor, the prefactor being proportional to the true line strength of that transition and the population factor being determined by Boltzmann statistics for the corresponding initial energy level. The prefactors can be found—at least approximately—by fitting the integral's temperature dependence. The result is shown in figure 11. Although the smooth change with temperature of Boltzmann population factors and uncertainties in the evaluation of the integrated cross section render a unique fit impossible, the best fits are obtained for line strengths of the transition beginning at 188 cm^{-1} about three times that of the transition beginning at 90 cm^{-1}. The transition beginning at 277 cm^{-1} contributes very little to the integral, and indeed a satisfactory fit can be achieved by neglecting it altogether.

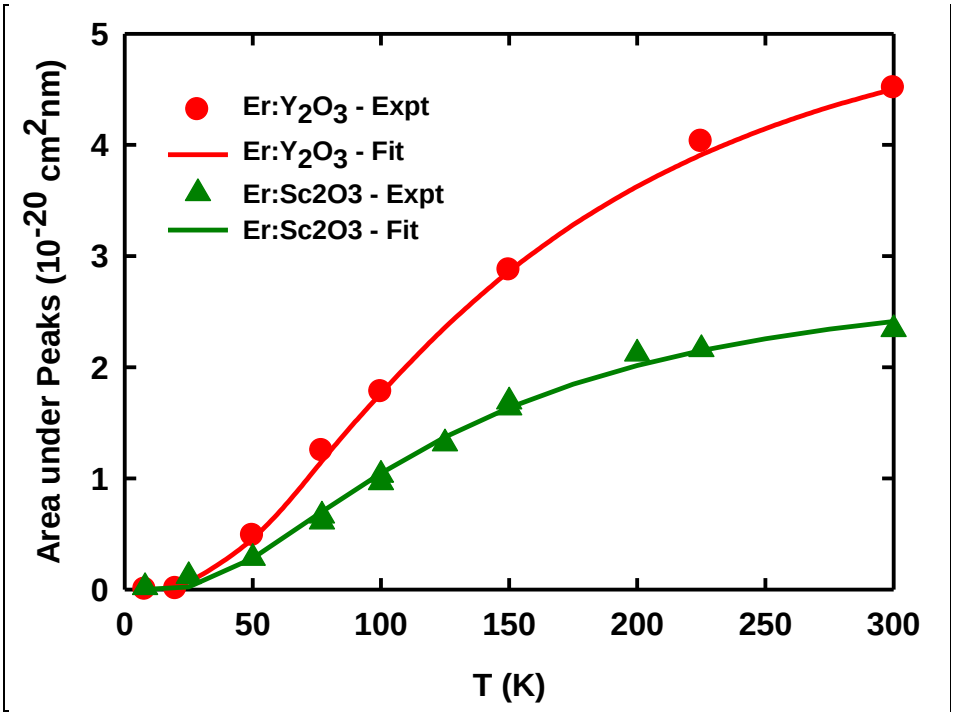

Figure 11. Temperature dependence of the integral over wavelength of the absorption cross section of the lines near 1550–1560 nm. The green symbols are Er:Sc_2O_3 integrals and the red symbols are Er:Y_2O_3 integrals. The green and red curves are the respective fits to a sum of thermal population terms, one term for each initial state involved in the set of overlapping transitions.

No such overlap of transitions affects the laser line at 1581 nm. It is weaker at 77 K than the total peak at 1558 nm, but has so much lower absorption that it can reach laser threshold first if the output coupling is chosen appropriately. However, as the temperature is increased, and without thermal population of higher states to add to its strength, thermal broadening reduces the

1581-nm line's gain cross section over a temperature range in which thermal population keeps the gain at 1558 nm approximately constant.

It is thus this much stronger transition involving higher-lying initial and final states that explains why thermal population at increasing temperatures actually favors 1558-nm lasing as the temperature is raised somewhat above 77 K.

It is of interest to calculate and fit the temperature dependence of the analogous cross-section integral for Er:Y_2O_3. In this case, there are four initial states and thus four terms in the sum of transition strengths, making the uncertainty in the fitting considerably worse. The result, also shown in figure 11, indicates only that satisfactory fits require all four initial levels, (in contrast to the situation in Er:Sc_2O_3,) and that the line strengths of the transitions initiating on the 158- and 258-cm^{-1} levels in figure 9 must be several times as strong as those initiating on the 76- and 89-cm^{-1} levels.

This result suggests that lasing Er:Y_2O_3 on the peak at 1553.5 or 1556.5 nm may be favored even more strongly with increasing temperatures than is the 1558-nm line in Er:Sc_2O_3. However, the energy differences between these lines and the zero line of Er:Y_2O_3 are smaller than that of Er:Sc_2O_3. Although this gives the Er:Y_2O_3 transitions even smaller quantum defects, it also makes the ratio of stimulated emission to absorption cross sections less favorable (just as was noted earlier in comparing the Er:Y_2O_3 1574-nm line to the Er:Sc_2O_3 1581-nm line). This may well erase any practical advantage of Er:Y_2O_3. Due to the limited optical quality of the available Er:Y_2O_3 samples, we have not been able to make a comparison of the two materials' laser properties.

7. Width and Structure of the Zero Line in Er:Sc_2O_3, Er:Y_2O_3, and Er:YAG

Minimizing the quantum defect in a pump-lase scheme calls for using the longest wavelength strong absorption line that is available, but as figures 2, 4, 6, and 7 indicate, that line tends to be quite narrow at 77 K. As a result, efficient absorption of the light from a pump laser diode can require that the diode be spectrally narrowed quite aggressively. This adds cost and generally reduces diode efficiently, so that it is of value to investigate the zero line of each laser material.

The zero line of Er:YAG, at 1532 nm, is the narrowest of the materials considered in this study. Indeed, at 77 K, the available spectrometers do not have sufficient resolution to give a reliable value, leading us to use the tunable external cavity diode laser noted in the experimental methods section. Measuring its transmission as the wavelength is tuned and then calculating the absorption cross section, the resulting full width at half maximum of the peak is 0.023 nm at 77 K. Its temperature dependence is given in figure 12, which combines diode laser scans at the lowest temperatures with spectrophotometer scans at temperatures for which that instrument's resolution is sufficient.

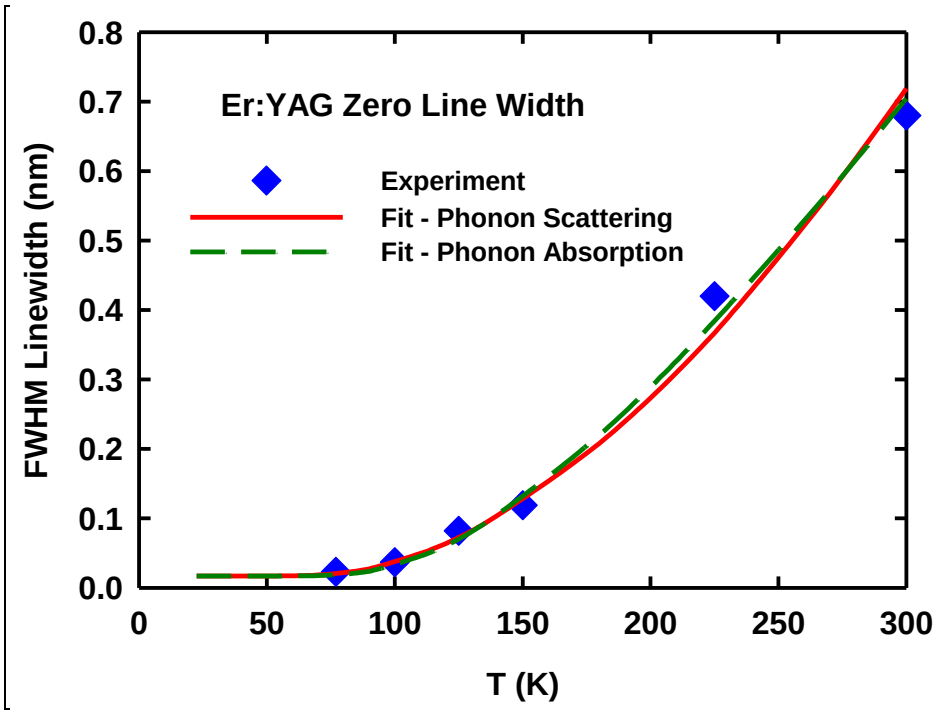

Figure 12. Temperature dependence of the Er:YAG zero-line width. The diamonds are the experimental data the solid curve is the fit by phonon scattering, and the dashed curve is the fit by phonon absorption.

The most common mechanisms for thermal broadening of spectral lines in solids are phonon emission, phonon absorption, and phonon scattering. The equations for the resulting temperature dependences are as follows, assuming for simplicity that one transition dominates the processes of phonon emission and phonon decay (*35*).

$$\Delta\lambda_{FWHM}(\text{phonon emission}) = A/(\exp(\hbar\omega_0/k_BT) - 1) \quad (3)$$

$$\Delta\lambda_{FWHM}(\text{phonon absorption}) = A\times\exp(\hbar\omega_0/k_BT)/(\exp(\hbar\omega_0/k_BT) - 1) \quad (4)$$

$$\Delta\lambda_{FWHM}(\text{phonon scattering}) = A\times(T/T_D)^7\times\int(x^6\exp(x)/(\exp(x) - 1)^2)dx \quad (5)$$

Here $\Delta\lambda_{FWHM}$ is the full width at half maximum of the peak, $\hbar\omega_0$ is the energy difference between the initial state and the final state reaches by the emission or absorption of a phonon, k_B is Boltzmann's constant, T is the absolute temperature, T_D is the Debye temperature of the material, the integral is over the interval 0 to (T_D/T), and A is a constant. Exploration shows that phonon emission cannot fit the observed temperature dependence, perhaps not surprisingly, since the zero line is an optical transition between the lowest level of each manifold. Both phonon absorption and phonon scattering can give a satisfactory fit, particularly if a small (0.017 nm) temperature-independent inhomogeneous linewidth is added to each fitting. The T_D value needed to get a good fit via phonon scattering is about 450 K, in reasonable agreement with the 405 K reported by Beghi et al. from fitting other transitions in this material (*36*). The transition energy required for a fit via phonon absorption is also about 450 K in temperature units, hence

313 cm^{-1}. This does not correspond any energy spacing between levels of either the $^4I_{15/2}$ or $^4I_{13/2}$ manifold of Er:YAG. If phonon absorption does control the thermal broadening, it must involve the sum of transitions to several final states, with similar enough strengths to give an effective value of $\hbar\omega_0$ that is not near any individual energy. By Occam's Razor, the greater simplicity and physically reasonable fitting parameter of the phonon scattering model make it the preferred interpretation.

Regardless of the line broadening mechanism, the very narrow linewidth of the Er:YAG zero line at 77 K makes it more difficult to use this line efficiently for diode pumping of a cryogenic laser. It is this narrowness that makes the weaker but much broader absorption feature at 1546 nm competitive as a pump line, as noted in a previous section.

Both Er:Sc_2O_3 and Er:Y_2O_3 exhibit much broader linewidths at 77 K in the zero-line region, 0.32 and 0.19 nm, respectively. Even at 8 K, the width in Er:Sc_2O_3 is 0.26 nm—still an order of magnitude greater than in Er:YAG. (For Er:Y_2O_3 at 8 K, the observed width of 0.12 nm may well be instrument limited.)

These greater linewidths can facilitate diode pumping, but some potential causes for such breadth would negate their advantages. The Er:Sc_2O_3 zero line is seen in absorption in figure 13 and that of Er:Y_2O_3 is shown in figure 14. The very substantial width of the Er:Sc_3O_3 line raises the possibility of inhomogeneous broadening. This would be undesirable, as it has the effect of diluting the effective cross section (or equivalently of reducing the concentration of ions that absorb or emit at any one wavelength). Indeed, figures 4 and 6 show that at 77 K the absorption and emission peaks of Er:Sc_2O_3 generally are broader and somewhat weaker than the corresponding peaks of Er:Y_2O_3. However, inhomogeneous broadening typically results in a Gaussian line shape, whereas the observed shapes in figures 13 and 14 are much more nearly Lorentzian. Thus, other mechanisms should be sought. The generally broader linewidths in Er:Sc_2O_3 may be due in part to the fact that Sc_2O_3 has a significantly larger maximum phonon energy than does Y_2O_3, which can promote all nonradiative processes (*37*).

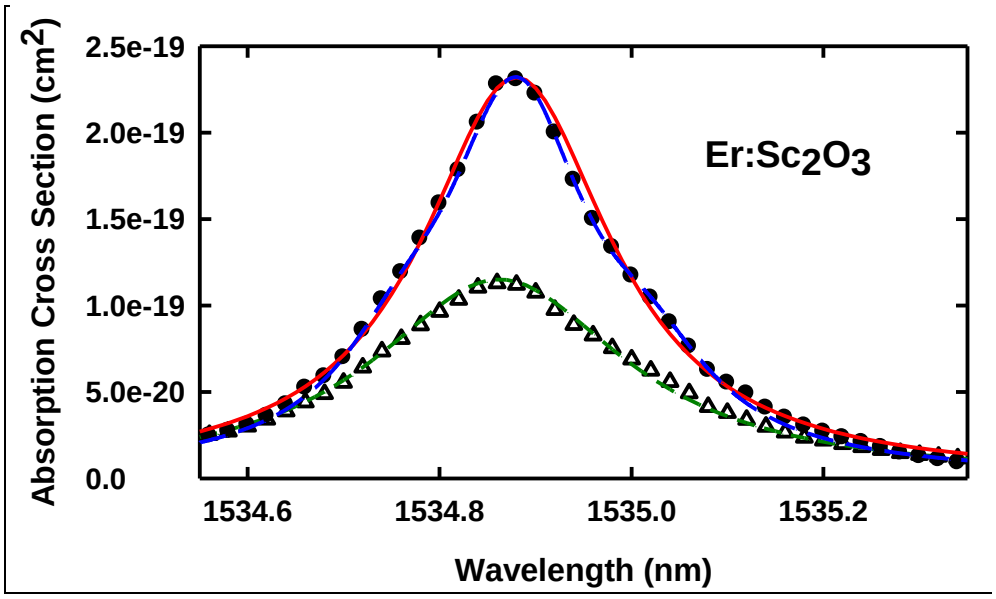

Figure 13. Zero-line absorption of $Er:Sc_2O_3$ at low temperatures. The filled symbols are experimental data at 8 K. the red curve is the single-peak fit at 8 K, the blue dashed curve is the three-peak fit at 8 K, the open symbols are experimental data at 77 K, and the green dashed curve is the single-peak fit at 77 K.

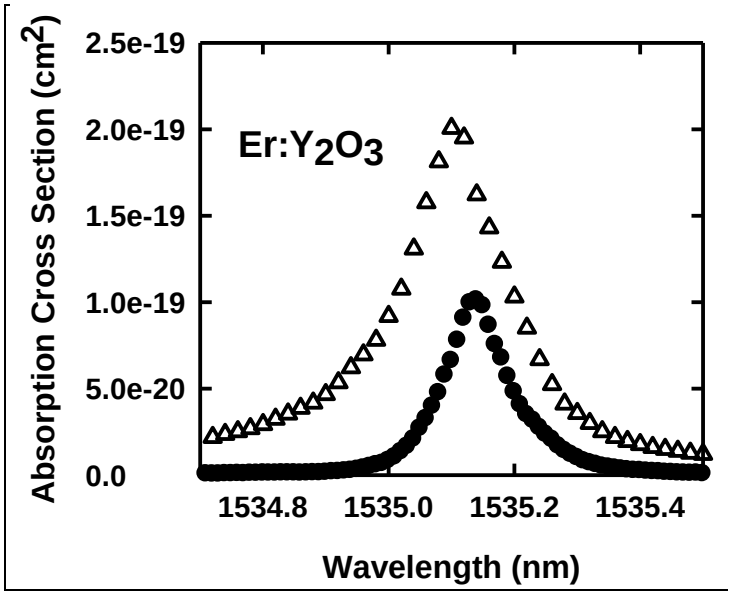

Figure 14. Zero-line absorption of $Er:Y_2O_3$ at low temperatures. The filled symbols are experimental data at 8 K and the open symbols are experimental data at 77 K.

For the zero line specifically, the detailed shape of the 8 K spectrum in figure 13 provides a clue. The peak is not fit quite adequately by a single Lorentzian line shape and is fit much better by three Lorentzians with somewhat different center wavelengths. Thus, a significant amount of the observed breadth is due to this distribution of lines. (This effect is also detectable in the 77 K

data, as shown in figure 13, but due to the thermal broadening of each line the three-line structure is much subtler.) The energy level diagram of Er^{3+} in the C_2 site of Sc_2O_3 (figure 9) does not show persuasive evidence of multiple transitions at the same energy as the zero line. The transition between the second levels of the $^4I_{15/2}$ and $^4I_{13/2}$ manifolds differs from the zero line by more than a nanometer, far more than the differences among the three overlapping peaks at the zero-line position. There is a transition at the same energy between states 90 cm^{-1} above the bottom of each manifold, but thermal population of an initial state that high is negligible at 8 K. Thus, it is more plausible that the additional two transitions at the zero-line energy are from Er^{3+} in other sites—possibly the C_{3i} site or a defect-perturbed site. This means that inhomogeneous broadening may indeed be responsible for the width of the zero line at very low temperatures, but in this case it is discrete broadening due to a few different sites, rather than the many random sites more often envisioned when inhomogeneous broadening is invoked.

The likelihood that the breadth of the zero line is due to more than one site raises concerns regarding that width's potential to facilitate efficient diode pumping. If excited Er^{3+} ions on the different sites transfer energy among the sites rapidly, pumping multiple sites can contribute to laser efficiency. Similarly, if all three sites' emission lines at the laser wavelength overlap sufficiently, all may contribute to laser gain, again leading to high efficiency. However, if their gain lines do not overlap sufficiently well and energy transfer among them is poor, the absorption of pump light by the sites not giving the maximum gain may be wasted. Investigation of this matter is under way.

The zero line in Er:Y_2O_3 is narrower than in Er:Sc_2O_3, as figure 14 shows. However, its strength and width grow with temperature in a promising way. The energy levels of Er^{3+} in the C_2 site in Y_2O_3 (figure 9) show an absorption transition beginning at 76 cm^{-1} that is at only slightly shorter wavelength than the zero line. That level's thermal population is negligible at 8 K, but is about one quarter that of the ground state by 77 K. Thus, that transition may well be responsible for the growth and blue shift of the zero line between those two temperatures. This is intriguing, because it would mean that both transitions contributing to the absorption at 77 K are in ions on the same site, and thus both can contribute straightforwardly to population of the upper laser level. It also means that the absorption at this wavelength can be expected to get still stronger as the temperature is raised above 77 K, as can be expected in a realistic high power cryogenic laser scheme.

8. Summary and Conclusions

We have compared the general properties of the $^4I_{15/2} \leftrightarrow {}^4I_{13/2}$ spectra of Er:YAG, Er:Y_2O_3, Er:Sc_2O_3, and (briefly) Er:Lu_2O_3. We have also addressed a few more detailed features of that spectroscopy that bear on laser operation, particularly at cryogenic temperatures. These details involve the longest-wavelength transition of Er:YAG among those on the short-wavelength side

of the large gap in its 77 K spectra, the unusual temperature dependence of lines in Er:Sc_2O_3 and Er:Y_2O_3 that are favorable for very small quantum defect lasing at cryogenic temperatures, and the widths of the zero lines in each material at 77 K, with reference to their use for diode pumping.

It seems quite clear that Er:YAG is the best material of this group for room-temperature laser operation in the 1.5–1.6 micron region. At that temperature, only relatively long wavelength emission lines (beyond about 1600 nm) have weak enough absorption to have usefully low laser thresholds, and Er:YAG has peaks in that region with much larger stimulated emission cross sections than do the Er-doped sesquioxides. Even though the sesquioxides have somewhat better thermal conductivity, it is difficult to overcome the large spectroscopic advantage held by YAG.

For cryogenic laser operation, in particular at or near liquid nitrogen temperature, the situation is nearly reversed. If one wishes to accept the same moderately small quantum defect as at room temperature, then Er:YAG remains the better choice for the same reasons, but the energy level structures give Er-doped sesquioxides a potential for very small quantum defect laser operation that Er:YAG lacks.

It is much more difficult to state which of the Er-doped sesquioxides is most favorable for cryogenic lasing. Due to the availability of sufficient data and analysis, we must limit the comparison to Er:Y_2O_3 and Er:Sc_2O_3. As a practical matter, we have observed better success with Er:Sc_2O_3, but this due to the optical quality of available samples, not to intrinsic properties. Er:Sc_2O_3 has a broader linewidth for pumping the longest wavelength strong absorption line, but that breadth may not be fully usable if the added lines that give that width are due to Er in different sites. The single-site nature of the strongest absorption lines of Er:Y_2O_3 at the zero-line wavelength, and the growth of one of those lines with temperature, make it much more promising for pumping than the linewidth alone would suggest.

The crystal field splitting of Er:Sc_2O_3 is generally smaller than that of Er:Y_2O_3, with the result that for analogous transitions Er:Y_2O_3 offers a somewhat smaller quantum defect but also has more ground state absorption to overcome to reach laser threshold. The transitions in Er:Y_2O_3 are generally narrower with higher peak stimulated emission cross sections. If one is willing to accept somewhat larger quantum defect one can use, for example, the Er:Y_2O_3 1574-nm line rather than the Er:Sc_2O_3 1558-nm line to get a lower threshold, while securing a slightly better quantum defect and stimulated emission cross section than with the Er:Sc_2O_3 1581-nm line.

Indeed, because the potentially useful emission lines of Er in these two hosts are staggered in wavelength, one has considerable freedom to explore the trade-off between small quantum defect (often accompanied by larger gain) and low absorption (a factor in achieving low laser threshold). Rather, one will have this flexibility when appropriately sized pieces of both materials are available with comparably high optical quality.

9. References

1. Aggarwal, R. L.; Ripin, D. J.; Ochoa, J. R.; Fan, T. Y. Measurement of Thermo-optic Properties of $Y_3Al_5O_{12}$, $Lu_3Al_5O_{12}$, $YAlO_3$, $LiYF_4$, $LiLuF_4$, BaY_2F_8, $KGd(WO_4)_2$, and $KY(WO_4)_2$ Laser Crystals in the 80–300 K Temperature Range. *J. Appl. Phys.* **2005**, *98*, 103514.

2. Zuclich, J. A.; Gagliano, D. A.; Cheney, F.; Stuck, B. E.; Zwick, H.; Edsall, P.; Lund, D. J. Ocular Effects of Penetrating IR Laser Wavelengths. *SPIE* **1995**, *2391*, 112–125.

3. Merkle, L. D.; Newburgh, G. A.; Ter-Gabrielyan, N.; Michael, A.; Dubinskii, M. Temperature-dependent Lasing and Spectroscopy of Yb:Y_2O_3 and Yb:Sc_2O_3. *Opt. Commun.* **2008**, *281*, 5855–5861.

4. Ter-Gabrielyan, N.; Merkle, L. D.; Ikesue, A.; Dubinskii, M. Ultralow Quantum-defect Eye-safe Er:Sc_2O_3. *Opt. Lett*. **2008**, *33* (13), 1524–1526.

5. Ter-Gabrielyan, N.; Dubinskii, M.; Newburgh, G. A.; Michael, A.; Merkle, L. D. Temperature Dependence of a Diode-pumped Cryogenic Er:YAG Laser. *Opt. Expr.* **2009**, *17* (9), 7159–7169.

6. Newburgh, G. A.; Word-Daniels, A.; Michael, A.; Merkle, L. D.; Ikesue, A.; Dubinskii, M. Resonantly Diode-pumped Ho^{3+}:Y_2O_3 Ceramic 2.1 μm Laser. *Opt. Expr.* **2011**, *19* (4), 3604–3611.

7. Klein, P. H.; Croft, W. J. Thermal Conductivity, Diffusivity, and Expansion of Y_2O_3, $Y_3Al_5O_{12}$, and LaF_3 in the Range 77–300 K. *J. Appl. Phys.* **1967**, *38* (4), 1603–1607.

8. Fan, T. Y.; Ripin, D. J.; Aggarwal, R. L.; Ochoa, J. R.; Chann, B.; Tilleman, M.; Spitzberg, J. Cryogenic Yb^{3+}-doped Solid-state Lasers. *IEEE J. Sel. Topics Quantum Electron.* **2007**, *13* (3), 448–459.

9. Wyckoff, R.W.G. *Crystal Structures,* vol. 2, 2nd ed.; Interscience: New York, 1964, pp 2ff.

10. Chang, N. C.; Gruber, J. B.; Leavitt, R. P.; Morrison, C. A. Optical Spectra, Energy Levels, and Crystal-field Analysis of Tripositive Rare Earth Ions in Y_2O_3. I. Kramers ions in C_2 sites. *J. Chem. Phys.* **1982**, *76* (8), 3877–3889.

11. Gruber, J. B.; Leavitt, R. P.; Morrison, C. A.; Chang, N. C. Optical Spectra, Energy Levels, and Crystal-field Analysis of Tripositive Rare Earth Ions in Y_2O_3. IV. C_{3i} Sites. *J. Chem. Phys.* **1985**, *82* (12), 5373–5378.

12. Shannon, R. D. Revised Effective Ionic Radii and Systematic Studies of Interatomic Distances in Halides and Chalcogenides. *Acta Cryst.* **1976**, *A32*, 751–767.

13. Payne, S. A.; Chase, L. L.; Smith, L. K.; Kway, W. L.; Krupke, W. F. Infrared Cross-section Measurements for Crystals Doped with Er^{3+}, Tm^{3+}, and Ho^{3+}. *IEEE J. Quantum Electron.* **1992**, *28* (11), 2619–2630.

14. Aull, B. F.; Jenssen, H. P. Vibronic Interactions in Nd:YAG Resulting in Nonreciprocity of Absorption and Stimulated Emission Cross Sections. *IEEE J. Quantum Electron.* **1982**, *QE-18* (5), 925–930.

15. Zelmon, D. E.; Small, D. L.; Page, R. Refractive-index Measurements of Undoped Yttrium Aluminum Garnet from 0.4 to 5.0 µm. *Appl. Opt.* **1998**, *37* (21), 4933–4935.

16. *Handbook of Optics*, Vol IV, 3rd edition, ed. M. Bass, C. DeCusatis, G. Li, V. N. Mahajan and E. Van Stryland (McGraw-Hill, 2009).

17. Mix, E. *Kristallzuohtung, Spektroskopie un Lasereingenschaften Yb-dotierter Sesquioxide*, dissertation, Institut fur Laser-Physik, U. Hamburg (1999).

18. Medenbach, O.; Dettmar, D.; Shannon, R. D.; Fischer, R. X.; Yen, W. M. Refractive Index and Optical Dispersion of Rare Earth Oxides using a Small-prism Technique. *J. Opt. A: Pure Appl. Opt.* **2001**, *3*, 174–177.

19. Merkle, L. D.; Ter-Gabrielyan, N. Cross Sections for Room and Low Temperature Operation of Er-Doped Sesquioxide Lasers. *Conference on Lasers and Electro-Optics 2007*, paper CThDD1.

20. Spariosu, K.; Birnbaum, M. Intracavity 1.549-µm Pumped 1.634-µm Er:YAG Lasers at 300 K. *IEEE J. Quantum Electron.* **1994**, *30* (4), 1044–1049.

21. Young, Y. E.; Setzler, S. D.; Snell, K. J.; Budni, P. A.; Pollak, T. M.; Chicklis, E. P. Efficient 1645-nm Er:YAG Laser. *Opt. Lett.* **2004**, *29* (10), 1075–1077.

22. Garbuzov, D.; Kudryashov, I.; Dubinskii, M. Resonant Diode Laser Pumped 1.6-µm-erbium-doped Yttrium Aluminum Garnet Solid-state Laser. *Appl. Phys. Lett.* **2005**, *86*, 131115.

23. Setzler, S. D.; Francis, M. P.; Young, Y. E.; Konves, J. R.; Chicklis, E. P. Resonantly Pumped Eyesafe Erbium Lasers. *IEEE J. Sel. Topics Quantum Electron.* **2005**, *11* (3), 645–657.

24. Garbuzov, D.; Kudryashov, I.; Dubinskii, M. 110 W(0.9 J) Pulsed Power from Resonantly Diode-laser-pumped 1.6-µm Er:YAG Laser. *App. Phys. Lett.* **2005**, *87*, 121101.

25. Setzler, S. D.; Francis, M. W.; Chicklis, E. P. A 100 mJ Q-switched 1645 nm Er:YAG Laser. *SPIE Defense and Security Symposium*, paper 6552-17, 2007.

26. Kim, J. W.; Shen, D. Y.; Sahu, J. K.; Clarkson, W. A. High-power In-band Pumped Er:YAG Laser at 1617 nm. *Opt. Expr.* **2008**, *16* (8), 5807–5812.

27. Gruber, J. B.; Quagliano, J. R.; Reid, M. F.; Richardson, F. S.; Hills, M. E.; Seltzer, M. D.; Stevens, S. B.; Morrison, C. A.; Allik, T. H. Energy Levels and Correlation Crystal-field Effects in Er^{3+}-doped Garnets. *Phys. Rev. B* **1993**, *48* (21), 15,561–15,573.

28. Gruber, J. B.; Nijjar, A. S.; Sardar, D. K.; Yow, R. M.; Russell III, C. C.; Allik, T. H.; Zandi, B. Spectral Analysis and Energy-level Structure of $Er^{3+}(4f^{11})$ in Polycrystalline Ceramic Garnet $Y_3Al_5O_{12}$. *J. Appl. Phys.* **2005**, *97*, 063519.

29. Laversenne, L.; Goutaudier, C.; Guyot, Y.; Cohen-Adad, M. Th.; Boulon, G. Growth of Rare Earth (RE) Doped Concentration Gradient Crystal Fibers and Analysis of Dynamical Processes of Laser Resonant Transitions in RE-doped Y_2O_3 (RE=Yb^{3+}, Er^{3+}, Ho^{3+}). *J. Alloys and Comp.* **2002**, *341*, 214–219.

30. T. Y. Fan, private communication, 2006.

31. Ter-Gabrielyan, N.; Fromzel, V.; Merkle, L. D.; Dubinskii, M. Resonant In-band Pumping of Cryo-cooled Er^{3+}:YAG Laser at 1532, 1534, and 1546 nm: A Comparative Study. *Opt. Mater. Expr.* **2011**, *1* (2), 223–233.

32. Ter-Gabrielyan, N.; Fromzel, V.; Dubinskii, M. Performance Analysis of the Ultra-low Quantum Defect Er^{3+}:Sc_2O_3 Laser. *Opt. Mater. Expr.* **2011**, *1* (3), 503–513.

33. Merkle, L.; Ter-Gabrielyan, N.; Cote, K. Er^{3+} in Sc_2O_3 and Y_2O_3: Spectroscopy to Elucidate Laser Behavior. *International Conference on Luminescence 2011*, paper ThII1.

34. Lupei, A.; Lupei, V.; Gheorghe, C.; Ikesue, A. Excited States Dynamics of Er^{3+} in Sc_2O_3 Ceramic. *J. Lumin.* **2008**, *128*, 918–920.

35. Powell, R. C. *Physics of Solid-State Laser Materials*; Springer: New York, 1998, p 143.

36. Beghi, M. G.; Bottani, C. E.; Russo, V. Debye Temperature of Erbium-doped Yttrium Aluminum Garnet from Luminescence and Brillouin Scattering Data. *J. Appl. Phys.* **2000**, *87* (4), 1769–1774.

37. Peters, V. *Growth and Spectroscopy of Ytterbium-Doped Sesquioxides*, dissertation, University of Hamburg, Germany, 2001.

List of Symbols, Abbreviations, and Acronyms

η	quantum efficiency of the emission
λ	wavelength
ω_0	angular frequency
σ_a	absorption cross section
τ_f	fluorescence lifetime
$\tau_{radiative}$	radiative lifetime
σ_{se}	stimulated emission cross section
$\Delta\lambda_{FWHM}$	full width at half maximum width of a spectral line or peak
c	speed of light in vacuum
ARL	U.S. Army Research Laboratory
CW	continuous wave
E_0	zero line energy
Er	erbium
Er^{3+}	trivalent erbium
F-L	Fuchtbauer-Ladenburg
GSA	ground-state absorption
h	Planck's constant
$\hbar$	Planck's constant divided by 2π
$\hbar\omega_0$	energy difference between two states
Ho	holmium
Ho^{3+}	trivalent holmium
I	intensity
InGaAs	indium gallium arsenide
k_B	Boltzmann's constant
Lu	lutetium
Lu_2O_3	lutetium oxide

n	index of refraction
nIR	near infrared
Sc	scandium
Sc_2O_3	scandium oxide
SE	stimulated emission
T	temperature
T_D	Debye temperature
Ti	titanium
UV	ultraviolet
vis	visible
Y	yttrium
Y_2O_3	yttrium oxide
YAG	yttrium aluminum garnet
Yb	ytterbium
Yb^{3+}	trivalent ytterbium
Z_l	partition function for the lower manifold
Z_u	partition function for the upper manifold

1 (PDF only) DEFENSE TECHNICAL INFORMATION CTR
DTIC OCA
8725 JOHN J KINGMAN RD
STE 0944
FORT BELVOIR VA 22060-6218

1 DIRECTOR
US ARMY RESEARCH LAB
IMNE ALC HRR
2800 POWDER MILL RD
ADELPHI MD 20783-1197

1 DIRECTOR
US ARMY RESEARCH LAB
RDRL CIO LL
2800 POWDER MILL RD
ADELPHI MD 20783-1197

1 DIRECTOR
US ARMY RESEARCH LAB
RDRL CIO MT
2800 POWDER MILL RD
ADELPHI MD 20783-1197

9 US ARMY RSRCH LAB
ATTN RDRL SEE M M DUBINSKIY
ATTN RDRL SEE M V FROMZEL
ATTN RDRL SEE M L MERKLE
(5 COPIES)
ATTN RDRL SEE M A MICHAEL
ATTN RDRL SEE M N TER-GABRIELYAN
ADELPHI MD 20783-1197

2 US ARMY SMDC
ATTN SMDC RDT DD K KENDRICK
ATTN SMDC RDT DD A ABERLE
HUNTSVILLE AL 35807

1 DR JOHN B GRUBER
5870 MEANDER DRIVE
SAN JOSE CA 95120-3839

2 DR DHIRAJ SARDAR
DR KELLY NASH
DEPARTMENT OF PHYSICS AND ASTRONOMY
UNIVERSITY OF TEXAS AT SAN ANTONIO
ONE UTSA CIRCLE
SAN ANTONIO TX 78249